

**V474 Car: A Rare Halo RS CVn Binary in Retrograde Galactic Orbit**

Eric J. Bubar, Eric E. Mamajek

*University of Rochester, Department of Physics & Astronomy, Rochester, NY, 14627-0171, USA*

Eric L. N. Jensen

*Swarthmore College, Department of Physics & Astronomy, 500 College Avenue, Swarthmore, PA 19081, USA*

Frederick M. Walter

*Department of Physics & Astronomy, Stony Brook University, Stony Brook, NY 11794-3800***ABSTRACT**

We report the discovery that the star V474 Car is an extremely active, high velocity halo RS CVn system. The star was originally identified as a possible pre-main sequence star in Carina, given its enhanced stellar activity, rapid rotation (10.3 days), enhanced Li, and absolute magnitude that places it above the main sequence. However, its extreme radial velocity ( $264 \text{ km s}^{-1}$ ) suggested that this system was unlike any previously known pre-MS system. Our detailed spectroscopic analysis of echelle spectra taken with the CTIO 4-m finds that V474 Car is both a spectroscopic binary with orbital period similar to the photometric rotation period, and metal poor ( $[\text{Fe}/\text{H}] \simeq -0.99$ ). The star's Galactic orbit is extremely eccentric ( $e \simeq 0.93$ ) with perigalacticon of only  $\sim 0.3$  kpc of the Galactic center - and its eccentricity and smallness of its perigalacticon are only surpassed by  $\sim 0.05\%$  of local F/G-type field stars. The observed characteristics are consistent with V474 Car being a high velocity, metal poor, tidally-locked chromospherically active binary (CAB), i.e. a halo RS CVn binary, and one of only a few such specimens known.

*Subject headings:* binaries: close – Galaxy: halo – stars: individual (V474 Car) – stars: activity – stars: kinematics – X-ray: binaries –

**1. Introduction**

In the course of a search for nearby pre-main-sequence stars among Hipparcos catalog stars with strong X-ray emission (Jensen et al. 2010), E. J. encountered the unusual star V474 Car

(HIP 44216, CPD-62 1150) which spectroscopically appeared to be remarkably similar to a G-type T Tauri star, with saturated X-ray emission and some  $H\alpha$  emission, but with a remarkably large radial velocity ( $v_r \simeq 250 \text{ km s}^{-1}$ ). As there were indications that this star might be a runaway T Tauri star, we conducted some follow-up observations to further characterize it.

There has been very little previous study of V474 Car. The star was listed as a high proper motion star ( $\mu \simeq 0''.2/\text{yr}$ ) multiple times by Luyten, and catalogued by Luyten (1979) as L 139-59, LTT 3338, and NLTT 20802. The star appeared in the 74th name list of variable stars as V474 Car (Kazarovets et al. 1999) and is entry ASAS 090023-6300.1 in the All Sky Automated Survey (ASAS) Catalog of Variable Stars (Pojmanski et al. 2005). The ASAS catalog lists V474 Car as a BY Dra-type star with a period of 10.312 days, V-band amplitude of 0.16 mag and maximum brightness of  $V = 9.94 \text{ mag}$ . Torres et al. (2006) listed V474 Car as SACY 525 in their spectroscopic survey of southern ROSAT X-ray sources, and classified the star as being a G0Ve star with large radial velocity ( $v_r = 247.8 \text{ km s}^{-1}$ ), slow projected rotation, but with lithium ( $\text{EW}(\text{Li I } \lambda 6707.8) = 100 \text{ m}\text{\AA}$ ), and weak  $H\alpha$  emission ( $\text{EW}(H\alpha) = -1.5 \text{ \AA}$ ). Hence, this star simultaneously shows paradoxical characteristics of both youth and old age.

Here we report our observations of the mysterious star V474 Car. We conclude that it is an extremely active, tight binary with an abundance pattern and space velocity consistent with belonging to the Galactic halo population. The photometric period for V474 Car matches the orbital period measured for the spectroscopic binary, confirming that V474 Car is a tidally-locked, active binary, i.e. an RS CVn system.

Table 1. Properties of V474 Car

Property	Value	Ref.
Parallax	$8.07 \pm 1.07$ mas	1
Distance	$124^{+19}_{-15}$ pc	1
RA(J2000)	09:00:23.24	1
Dec(J2000)	−63:00:04.3	1
$\mu_\alpha$	$114.54 \pm 0.93$ mas yr <sup>−1</sup>	1
$\mu_\delta$	$−111.79 \pm 0.99$ mas yr <sup>−1</sup>	1
V	10.24 mag	2
V <sub>max</sub>	9.94 mag	4
V <sub>mean</sub>	10.03 mag	4
J	$8.184 \pm 0.023$ mag	5
H	$7.626 \pm 0.042$ mag	5
K <sub>s</sub>	$7.470 \pm 0.026$ mag	5
B−V	$0.904 \pm 0.015$ mag	2
V−I <sub>C</sub>	$0.95 \pm 0.02$ mag	2
Period(phot)	10.30 days	2
...	10.312 days	4
Spec. Type	G0Ve	3
Soft X-ray flux	$0.195 \pm 0.025$ ct/s	6
...	$1.84 \pm 10^{-12}$ erg/s/cm <sup>2</sup>	6
HR1	$0.21 \pm 0.12$	6
HR2	$0.23 \pm 0.15$	6
L <sub>X</sub>	$10^{30.53}$ erg/s	6

Note. — References: (1) van Leeuwen (2007), distance is inverse of parallax, position is for epoch J2000 on ICRS, (2) Perryman et al. (1997), (3) Torres et al. (2006), (4) Pojmanski et al. (2005), (5) Cutri et al. (2003), (6) Voges et al. (1999), conversion to X-ray flux and luminosity using Fleming et al. (1995), and luminosity using parallax from van Leeuwen (2007). All

ROSAT X-ray fluxes are in the 0.1–2.4 keV band.

## 2. Observations

We took spectra of V474 Car with the 4-meter Blanco telescope at CTIO on 2001 April 7 and 2003 April 14, using the echelle spectrograph. The spectrograph covered a wavelength range from 4800 Å to 8400 Å with a measured spectral resolving power of  $R \sim 40,000$  and typical S/N $\sim$ 100-130. The spectra were reduced in IRAF<sup>1</sup> according to standard procedures. Observations of several radial velocity standards on each night indicates an overall radial velocity precision in high S/N spectra of better than 1 km s<sup>-1</sup>.

After noticing the large and variable radial velocity in the first two observations, we also monitored V474 Car with the spectrographs on the CTIO 1.5m telescope over a number of nights in April–June 2009 and January–February 2010.

We obtained 15 spectra with the echelle spectrograph<sup>2</sup>. The echelle, formerly on the Blanco 4m, is fiber-fed. The detector is a 2k SITe CCD with 24  $\mu$ m pixels. The full-chip readout gives coverage from 4020 to 7300Å at a resolving power of about 25,000 to 30,000 for the 100 and 130  $\mu$ m slits used. Integration times were typically 1 hour, in three 20 minute integrations, except on one night when we only took a single exposure. Data reduction utilized a basic echelle reduction package<sup>3</sup>.

We also obtained six low dispersion spectra using the long-slit RC spectrograph. These were used for spectral classification, to determine the stellar activity level, and to search for evidence of a cool companion. We used a 1.5 arcsec slit and four standard low dispersion spectroscopic setups (26/Ia, 47/Ib, 47/II, 58/I). We obtained three observations with integration times between 300 and 400 seconds, depending on the setup and the target brightness. The three observations were median-filtered to minimize contamination by cosmic rays. We reduced the data using our spectroscopic data reduction pipeline<sup>4</sup>.

## 3. Analysis

At first glance this star is puzzling, since it presents both pre-main-sequence characteristics and halo population characteristics. If the star is placed on an HR diagram, assuming that reddening corrections are negligible and that the secondary contributes little light in the  $V$  band, its position is consistent with a pre-main-sequence classification (and indeed this is why we initially selected it for observation). In addition, we measure modest H $\alpha$  emission (equivalent width =  $-1.25$  Å) and

---

<sup>1</sup>IRAF is distributed by the National Optical Astronomy Observatories, which are operated by the Association of Universities for Research in Astronomy, Inc., under cooperative agreement with the National Science Foundation.

<sup>2</sup><http://www.ctio.noao.edu/~atokovin/echelle/index.html>

<sup>3</sup>[http://www.astro.sunysb.edu/fwalter/SMARTS/smarts\\_15msched.html#ECHpipeline](http://www.astro.sunysb.edu/fwalter/SMARTS/smarts_15msched.html#ECHpipeline)

<sup>4</sup>[http://www.astro.sunysb.edu/fwalter/SMARTS/smarts\\_15msched.html#RCpipeline](http://www.astro.sunysb.edu/fwalter/SMARTS/smarts_15msched.html#RCpipeline)

find a lithium equivalent width from the  $\lambda 6707.8$  Li I line of  $91.1 \text{ m}\text{\AA}$ . All of these indicators are consistent with youth, which could imply that the star may be a “runaway” post-T Tauri star. However, the kinematics are also similar to that of halo stars. In order to clarify the status of this potentially interesting object, we now present a variety of analyses. We first discuss the kinematics, including disentangling the effects of binary orbital motion from those of overall space motion of the system. We then discuss the star’s X-ray emission, and we conclude this section with a high resolution spectroscopic abundance analysis.

### 3.1. Binary Orbit

Our first two observations, in 2001 and 2003, gave radial velocities differing by  $16 \text{ km s}^{-1}$ , suggesting that the system is a spectroscopic binary, so we made additional radial velocity observations. The measured velocities are given in Table 2. We fit the radial velocity data using the Binary Star Combined Solution software (Gudehus 2001) and our own custom-written IDL code; both gave the same solution.

The best-fit phased radial velocity curve is shown in Figure 1, and the orbital parameters are given in Table 3. The eccentricity is formally consistent with a circular orbit; forcing a circular orbit in the fit gives the same orbital parameters to within the uncertainties given in Table 3. In doing the fitting, we found that the three data points taken in January and February of 2010 were systematically low compared to the best-fit orbit. The camera for the spectrograph was removed from the dewar in December 2009, and we suspect that our reduction pipeline does not yet fully correct for a small rotation introduced when this change was made. Thus, we have applied an empirical  $+3.9 \text{ km s}^{-1}$  correction to those three datapoints, both in Table 2 and in the final orbital fit. However, even if we do not apply that correction, the orbital parameters are unchanged to within their quoted uncertainties.

The orbital fit yields a mass function of  $0.013 M_{\odot}$ , and thus this can also be used to place limits on the secondary mass. Based on our derived stellar parameters for the primary (Sec. 3.5), we interpolated Yale-Yonsei isochrones with a metallicity of our derived value ( $[\text{Fe}/\text{H}]=-0.97$ : discussed below) to yield an approximate primary mass of  $0.9 M_{\odot}$  (Demarque et al. 2004). As shown in Figure 2, this constrains the secondary mass to greater than  $0.25 M_{\odot}$ . Thus, it is likely to be a late K or M type companion, and it is plausible (especially for larger values of  $\sin i$ ) that we would not see any sign of it in our spectra.

We can place constraints on the inclination of the primary star’s rotation axis by comparing the inferred stellar rotation period with its projected equatorial rotational velocity  $v \sin i$  and also taking the star’s radius into account. The Yale-Yonsei isochrones (Demarque et al. 2004) yield an approximate primary stellar radius of  $1.9 R_{\odot}$ , which is consistent with a radius of  $1.5\text{--}2.0 R_{\odot}$  inferred from the Barnes-Evans relation (Barnes & Evans 1976) (uncertainty comes solely from parallax and neglects systematic metallicity or interstellar reddening effects). Combining this with

$P_{\text{rot}}$  and  $v \sin i$  (Table 4) suggests a high value for  $\sin i$  (within  $1.7\sigma$  of 1). Assuming that the stellar rotation axis is perpendicular to the binary orbit, this would imply a nearly edge-on orbit. Though no eclipses are evident in the photometric data, an edge-on orbit would give a companion mass of  $0.26 M_{\odot}$ . While Yale-Yonsei models do not go to this low of a mass, the lowest mass available in these models ( $0.40 M_{\odot}$ ) yield a secondary stellar radius of  $0.17 R_{\odot}$ . As a plausibility study, this would imply an eclipse depth of only 0.8 % ,which is undetectable given the existing photometry. It is worth noting however, given our derived secondary characteristics, that it is possibly a white dwarf.

### 3.2. Kinematics

Having determined the system’s center-of-mass radial velocity from the binary orbital solution, we can now investigate its three-dimensional kinematics more fully.

The proper motions for V474 Car from Perryman et al. (1997), Høg et al. (2000), van Leeuwen (2007), Röser et al. (2008), and Zacharias et al. (2010) are all within  $\pm 2 \text{ mas yr}^{-1}$  of each other. To estimate the Galactic Cartesian velocity for V474 Car, we combine the position, proper motion, and parallax from van Leeuwen (2007) with the systemic radial velocity estimated in §3.1. The resulting velocity is  $U, V, W = (137, -241, -41) \pm (10, 6, 3) \text{ km s}^{-1}$ , where  $U$  is pointed towards the Galactic center,  $V$  is in the direction of Galactic rotation ( $\ell, b = 90^{\circ}, 0^{\circ}$ ), and  $W$  is towards the North Galactic Pole ( $b = +90^{\circ}$ ). Note that the  $V$  velocity is almost directly opposite the Galactic rotational velocity of  $\sim 220 \text{ km s}^{-1}$  for disk stars in the solar neighborhood, indicating that V474 Car has a retrograde Galactic orbit with negligible rotational motion.

We used the *orbit* packages within the *NEMO: Stellar Dynamics Toolbox* (Teuben 1995) to integrate the orbit of this star in a model Galactic potential (potential 1 taken from Dehnen & Binney 1998). From these orbit integrations we find an average perigalacticon of 0.32 kpc and an apogalacticon of 9.20 kpc with an eccentricity of 0.93 and an orbital period of 202 Myr. Hence, we are catching V474 shortly after apogalacticon as it is “falling” towards the Galactic center (where it should pass within  $\sim 2.3$  of Sgr A\* during perigalacticon).

### 3.3. X-ray Emission

V474 Car is detected as an X-ray source (1RXS J090022.8–630012) in the ROSAT All-Sky Bright Source Catalog (RASS-BSC; Voges et al. 1999). While it is situated  $9''$  away from the optical star, the RASS X-ray source has an  $8''$  positional error, consistent with V474 Car being the optical counterpart. V474 Car is the brightest optical counterpart within  $112''$  of the X-ray source, and as V474 Car is clearly a chromospherically active, close binary, it is undoubtedly responsible for the X-ray emission. The X-ray counterpart was imaged over a total exposure time of 733 seconds on 14 June 1996, and has measured X-ray properties listed in Table 1. Using the RASS-BSC count rate

Table 2. Measured radial velocities

HJD	$v_r$ (km s $^{-1}$ )	$\sigma_v$ (km s $^{-1}$ )
2452006.59387	266.7	0.4
2452743.51096	282.8	0.3
2454958.60290	251.6	0.4
2454966.62641	279.9	0.4
2454969.49097	244.3	0.3
2454970.56424	240.9	0.3
2454971.51535	246.3	0.4
2454972.49168	258.1	0.4
2454973.51364	272.1	0.4
2454974.49883	282.9	0.4
2454985.50324	287.3	0.4
2454988.51663	260.4	0.2
2454993.52470	266.5	0.3
2455019.48989	254.8	0.3
2455201.71863	271.4 <sup>a</sup>	2.0
2455240.60836	287.0 <sup>a</sup>	0.3
2455243.66034	256.1 <sup>a</sup>	0.2

<sup>a</sup>Offset of +3.9 km s $^{-1}$  added; see text.

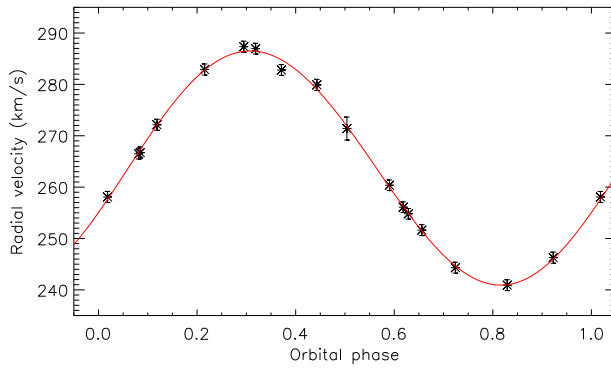


Fig. 1.— Phased radial velocity measurements of V474 Car, with the best-fit binary orbital solution ( $P = 10.1944$  days; solid line) superimposed.

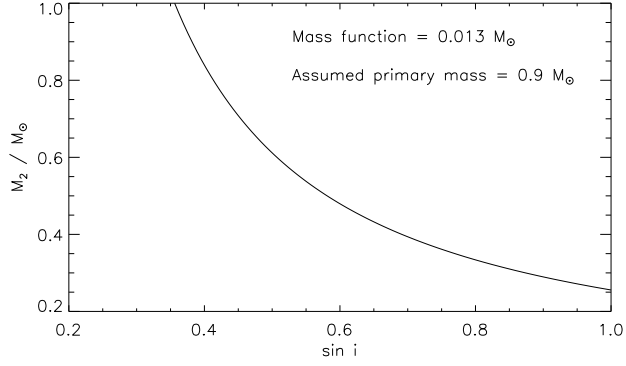


Fig. 2.— Constraints on the mass of the secondary star, assuming a primary mass of  $0.9 M_{\odot}$ .

Table 3. Spectroscopic Binary Solution

Property	Value
Systemic radial velocity $\gamma$	$263.8 \pm 0.3 \text{ km s}^{-1}$
Velocity semi-amplitude $K_1$	$22.8 \pm 0.5 \text{ km s}^{-1}$
$a_1 \sin i$	$0.0214 \pm 0.0005 \text{ AU}$
$e$	$0.014 \pm 0.018$
Period (days)	$10.1944 \pm 0.0003$

and HR1 hardness ratio, and the energy conversion factor equation of Fleming et al. (1995), we estimate the observed soft X-ray flux in the ROSAT passband (0.1-2.4 keV) of  $1.84 \pm 10^{-12}$  erg s $^{-1}$  cm $^{-2}$ . Combining the X-ray flux with the revised Hipparcos parallax from van Leeuwen (2007), we estimate the X-ray luminosity to be  $L_X = 10^{30.53}$  erg s $^{-1}$ . Through comparing the hardness ratios HR1 and HR2 for X-ray emitting coronal plasma models from Neuhäuser et al. (1995), V474 Car appears to have coronal temperatures of  $\sim 10$ – $17$  MK, with the X-ray flux likely observed through negligible interstellar absorption ( $N(H) < 10^{19}$  cm $^{-2}$ ). In comparing the hardness ratios HR1 and HR2 from Voges et al. (1999) for a sample of nearby RS CVn systems (Dempsey et al. 1993), we find that typical RS CVns have median values of HR1 = 0.03 ( $\pm 0.12$  ;  $1\sigma$ ) and HR2 = 0.16 ( $\pm 0.09$  ;  $1\sigma$ ). Comparing the hardness ratios for V474 Car listed in Table 1 with these mean values, we find that V474 Car’s X-ray colors are consistent (within the uncertainties) with those of other RS CVn systems. V474 Car’s hardness ratios are at the high end of the distribution, indicating relatively hot plasma. This may be due to the low metallicity of the system, which can inhibit efficient cooling of the coronal plasma (Fleming & Tagliaferri 1996).

### 3.4. Optical Variability

As noted in §1, the All Sky Automated Survey (ASAS) Catalog of Variable Stars (Pojmanski et al. 2005) show V474 Car to be variable with period 10.312 days, V-band amplitude of 0.16 mag, and maximum brightness of  $V = 9.94$  mag. This period is similar to the binary orbital period, suggesting that the stars’ rotation periods are tidally synchronized with the binary orbit. While the best-fit photometric period of 10.3 days is slightly longer than the binary orbital period of 10.2 days, it is still possible to reconcile the two periods with synchronized rotation if the dominant spots are at non-equatorial latitudes on the star and there is a modest amount of differential rotation.

When the 10-day period is removed from the light curve, a much longer term variation with an amplitude of  $\sim 0.2$  mag remains (Figure 3). The modulation appears to be roughly sinusoidal with a period of  $\sim 6$  years. Since the span of the data is only about 9 years it is not possible to tell if the variation is truly periodic. However, both the inferred period and amplitude are consistent with long-term activity cycles seen on other solar-type stars (Lockwood et al. 2007), suggesting that we may be observing the analog of our Sun’s 11-year magnetic activity cycle.

### 3.5. Spectroscopic Analysis

We utilized the echelle observations to derive a maximum projected rotational velocity. The  $v \sin i$  was determined from a calibration of cross-correlation peak width versus  $v \sin i$  for rotational velocity standards from Soderblom et al. (1989) (HD 165185 :  $7.0$  km s $^{-1}$ , HD 206860:  $10.2$  km s $^{-1}$ , HD 204121:  $18.5$  km s $^{-1}$ , HD 134083:  $45.0$  km s $^{-1}$ ). Macroturbulence is included inasmuch as it is equivalent to that in the standards. This allowed mapping a cross-correlation width to a  $v \sin i$ . The

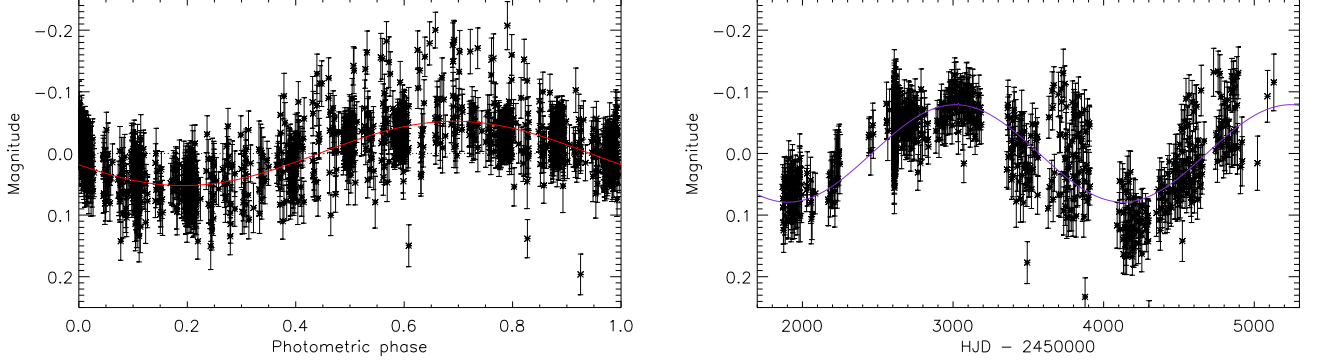


Fig. 3.— ASAS V-band photometry of V474 Car, showing the periodic variations. Top: Short-period variability, phased to  $P = 10.31$  days, similar to the binary orbital period. Bottom: Long-term variability, suggesting a solar-like magnetic activity cycle of  $\sim 6$  years. Each plot shows the data with the other period removed.

Table 4. Derived Parameters for V474 Car

Property	Value
$M_V$	4.56
Bolometric Correction	-0.22 (Flower 1996)
$M_{Bol}$	4.34
$Mass_{Primary}$	$0.90 \pm 0.02 M_{\odot}$
$Radius_{Primary}$	$1.90 \pm 0.94 R_{\odot}$
$Luminosity_{Primary}$	$2.69 \pm 0.77 L_{\odot}$
$T_{Excitation}$	$5238 \pm 152$ K
$\log g$	$3.64 \pm 0.51$
[Fe/H]	$-0.99 \pm 0.16$
Microturbulent Velocity	$2.52 \pm 0.44$ km s $^{-1}$
$v \sin i$	$11.8 \pm 3.0$ km s $^{-1}$
EW(Li I $\lambda 6707$ )	91 mÅ
EW(H $\alpha$ )	-1.25 Å

uncertainty from this calibration is of order 1.0 km/s. The more conservative uncertainty that we quote is estimated by taking the standard deviation in the  $v \sin i$  from the cross correlation peak width calibration across multiple orders for both epochs of echelle observations.

The ensuing spectroscopic abundance analysis has been performed differentially with respect to a solar spectrum obtained using the echelle spectrograph on the CTIO 4-m telescope. First, we examined the spectral features for any evidence of the secondary (asymmetry in cross correlation peaks, double lines). No such evidence was found. All lines were measured in both the solar and stellar spectrum and final abundances were found by subtracting solar abundances from stellar abundances in a line by line fashion. Unless otherwise noted, we quote all abundances in the standard bracket notation where  $[X/Y] = \log \frac{N(X)}{N(Y)}_{\text{stellar}} - \log \frac{N(X)}{N(Y)}_{\odot}$  and  $\log N(H) = 12$ .

We used 1-D plane-parallel model atmospheres interpolated from the ATLAS9 grids of Kurucz with an updated version of the LTE Spectral Synthesis tool MOOG (Snedden 1973) to derive abundances in a curve of growth approach from equivalent widths of spectral features. We use a high fidelity sample of 52 Fe I and 6 Fe II lines taken from Bubar & King (2010).

The temperature, surface gravity, microturbulent velocity ( $\xi$ ), and metallicity have been determined using the approach of excitation/ionization balance. The approach is commonly used for solar-type stars, and there is evidence that it is robust enough for application to our presumably RS CVn-like system (Morel et al. 2004). Briefly, the (excitation) temperature was found by adjusting the model atmosphere temperature to remove any correlation in  $[\text{Fe I}/\text{H}]$  versus excitation potential. The microturbulence was determined by adjusting microturbulence to remove any correlations between  $[\text{Fe I}/\text{H}]$  and line strength (i.e. reduced equivalent width). The surface gravity was found by forcing the abundance derived from singly ionized Fe lines to match that derived from neutral lines. With the availability of Hipparcos data, we were also able to obtain parallax-based physical surface gravities. We find the ionization-dependent gravity to be lower than this physical gravity ( $\log g_{\text{phys}}=4.15$ ). This is quantitatively similar to the differences between ionization balance and physical gravities observed by e.g. Fuhrmann (1998). Utilizing this gravity has a minimal effect on the quoted abundances (typically  $\pm 0.04$  dex). Within the uncertainties, this effect is negligible.

The spectroscopic parameters that we derive are  $T_{\text{exc}} = 5238 \pm 152$  K,  $\log g = 3.64 \pm 0.51$ ,  $[\text{Fe}/\text{H}] = -0.99 \pm 0.16$  and  $\xi = 2.52 \pm 0.44$  km s $^{-1}$ . We also derive oxygen abundances from the near-IR triplet, which is well known to be effected by significant NLTE effects. We interpolated within the grids of Ramírez et al. (2007) (using an IDL Spline3 interpolation routine kindly provided by Ivan Ramirez 2009, personal communication) to perform NLTE corrections and find a NLTE abundance. All other abundances have been derived from equivalent widths using the *abfind* driver of MOOG, with conservative uncertainties of order  $\pm 0.1$ – $0.2$  dex. Results are given in Table 5.

The derived abundances display a clear enhancement in  $[\alpha/\text{Fe}]$  (for the elements oxygen, magnesium, calcium and titanium  $< [\alpha/\text{Fe}] >= 0.35$ ) relative to the non- $\alpha$  abundances (Na, Mn, Ni, Y and Ba,  $< [X/\text{Fe}] >= -0.17$ ). The  $[\text{Si}/\text{Fe}]$  differs from the trends of the other  $\alpha$  elements, a result of uncertainties in the temperature and surface gravity. Moreover, the behavior is qualitatively

similar to  $\alpha$  enhancements observed in a sample of six halo RS CVn systems (Morel et al. 2004). Considering that the system is chromospherically active as implied by the H $\alpha$  emission, a variety of effects are likely at play and could explain the apparent enhancements. The presence of NLTE effects resulting in observational overexcitation/overionization (i.e. abundances derived from higher excitation potential lines and from lines of an ionized species are larger than their lower excitation potential and neutral counterparts) cannot be discounted. While there is no evidence that higher excitation potential lines or ionized lines yielded increased abundances in this star this may just be a manifestation of the excitation/ionization balance approach employed. Perhaps one of the most likely physical mechanisms that are impacting the abundance determinations above is the presence of significant photospheric inhomogeneities. Analytic spot models have been utilized by Schuler et al. (2006) to plausibly explain observational overexcitation and overionization in young open cluster dwarfs. Attempting to account for these effects is beyond the scope of this paper and therefore, we recommend exercising caution in more detailed interpretations of the abundance results.

However, for our purposes, we can conclude that the observed abundance signatures (neglecting lithium, which is discussed below) are at least qualitatively similar to those found by Morel et al. (2004), using a comparable approach. This provides compelling, though clearly not definitive, evidence that this is indeed a halo RS CVn system.

We have also determined lithium abundances through spectral synthesis of the Li I resonance line, using an updated line list from King et al. (1997) and King (2009, personal communication). From spectra at two available epochs, we derived LTE abundances of  $\log N(\text{Li}) = 2.10 \pm 0.20$  and  $2.20 \pm 0.20$ , respectively, with the former being from the higher quality, higher S/N spectra (Figure ??). From the code of Carlsson et al. (1994), we determined NLTE corrections and find NLTE Li abundances of  $\log N(\text{Li}) = 2.17$  and  $2.26$ , respectively. This abundance is not inconsistent with lithium abundance measurements for other chromospherically active binaries which occupy a similar temperature range (i.e. Fig. 3a of Barrado y Navascues et al. 1997).

## 4. Discussion

### 4.1. Classification

We can rule out V474 Car being a W UMa contact binary, as its rotational and orbital periods (10 days) are significantly longer than the  $\sim 0.2$ – $1.2$  days typically measured for W UMa systems (Rucinski & Duerbeck 1997; Maceroni & van’t Veer 1996). Similarly, we can rule out V474 Car being a FK Com-type rapidly rotating active G/K giant, as they are typically single (i.e. no velocity variations), and have  $v \sin i \sim 100 \text{ km s}^{-1}$ . We can also rule out V474 Car being a BY Dra binary, as it is clear that the primary is an evolved star. Lastly, we can dismiss the idea that V474 Car is a high velocity T Tauri star. Despite its H $\alpha$  emission, strong X-ray emission, lower surface gravity than dwarf stars, and significant Li absorption, the velocity of V474 Car is clearly halo-like, and our

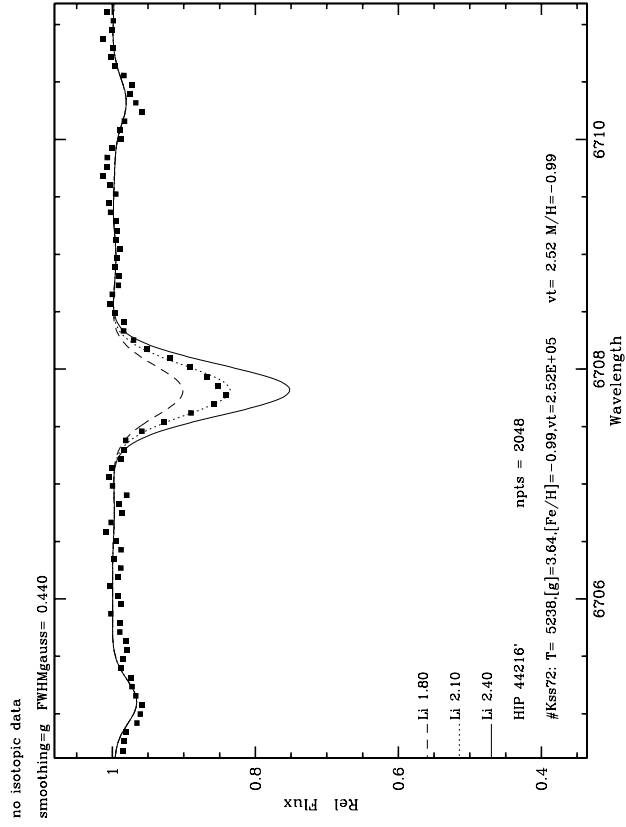


Fig. 4.— Lithium synthesis of the  $\lambda 6707$  doublet. A Gaussian function with a FWHM of 0.44 was used to smooth the synthetic spectrum, based on measurements of clean, weak lines in the spectrum. The figure shows the best fit lithium synthesis of  $\log N(\text{Li})=2.10$  from the higher S/N spectrum.

abundance analysis is consistent with the star being significantly metal poor ( $[\text{Fe}/\text{H}] \simeq -1.0$ ) with  $\alpha$  element enhancements reminiscent of other halo stars. Local T Tauri and other young stellar populations ( $< 100$  Myr) typically have metallicities near solar (e.g. Padgett 1996), and velocities within  $\sim 20 \text{ km s}^{-1}$  of the LSR (Makarov 2007). Given the match between the photometric and orbital period, we have reason to suspect that most of the indicators suggestive of youth ( $\text{H}\alpha$ , X-ray emission, starspots) are due to the system being a tidally-locked binary, rather than youth.

RS CVn systems are late-type, detached binary stars, with at least one component being evolved. RS CVns typically have rotation and orbital periods of  $\sim 3$ –20 days, are photometrically variable, and show strong chromospheric activity. V474 Car appears to satisfy all of these characteristics, and hence we classify the star as an RS CVn-type binary. RS CVns typically have  $v \sin i$  values in the tens of  $\text{km s}^{-1}$ , consistent with what we measure from our spectroscopic analysis (Table 4).<sup>5</sup>

#### 4.2. V474 Car: A Halo RS CVn System

A recent compilation by Eker et al. (2008) records  $\sim 400$  known chromospherically active binaries (CABs), with 164 explicitly classified as RS CVn systems. There are indications that V474 Car is fairly unusual compared to the majority of known RS CVn systems.

We cross-correlated all CABs in Eker et al. (2008) with the revised Hipparcos catalog and the compiled radial velocity catalog of Gontcharov (2006). We estimated Galactic Cartesian (UVW) velocities for all CABs with positive Hipparcos parallaxes and radial velocities in Gontcharov (2006). For those 251 CABs with velocities known to better than 50% accuracy, we find that V474 Car’s velocity ( $S = 280 \pm 7 \text{ km s}^{-1}$ ) exceeds the heliocentric velocity of *all* of these systems. The highest velocity star from Eker et al.’s compilation is HIP 81170 with  $S = 225 \pm 6 \text{ km s}^{-1}$ , the only HIP star in that catalog with velocity greater than  $200 \text{ km s}^{-1}$ .

Ottmann et al. (1997) conducted an X-ray survey of Population II, metal-poor binaries, and listed a sub-sample of 12 population II binaries showing significant chromospheric emission (in this case, the Ca H & K line). Combining the revised Hipparcos astrometry (van Leeuwen 2007) with the compiled radial velocity catalog of Gontcharov (2006), we calculated UVW velocities for these 12 emission-line Pop II binaries. We find that only two systems have heliocentric velocities greater than that of V474 Car: CD–48 1741 (HIP 24742) with  $S = 377 \pm 28 \text{ km s}^{-1}$ , and DR Oct (HD 89499, HIP 49616) with  $S = 376 \pm 22 \text{ km s}^{-1}$ . CD–48 1741 is arguably the most dynamically similar to V474 Car, with orbital period 7.56 days,  $[\text{Fe}/\text{H}] = -1.40$  (Spite et al. 1994), subgiant gravity for the primary ( $\log g = 4.00$ ; Spite et al. 1994), and retrograde Galactic orbit ( $V = -359 \pm 28 \text{ km s}^{-1}$ ). Despite its similarity to V474 Car in orbital period and distance, CD–48 1741 was not detected

---

<sup>5</sup>The value of  $v \sin i = 1.0 \pm 1.2 \text{ km s}^{-1}$  reported by Torres et al. (2006) is a typo and should be  $11.7 \text{ km s}^{-1}$  (C. Melo, personal communication, 2010).

in X-rays in the ROSAT All-Sky Survey, and its variability is much more subtle (no photometric period was reported in the Hipparcos catalog or in the AAVSO index). DR Oct is a single-lined spectroscopic binary with an evolved G-type primary, 5.57 day orbital period (Ardeberg & Lindgren 1991),  $[\text{Fe}/\text{H}] \simeq -2.2$  (Ryan & Deliyannis 1998; Snider et al. 2001), enhanced Li compared to halo dwarfs (Balachandran et al. 1993), and it appears to be the most metal-poor star to have its X-ray spectrum taken (Fleming & Tagliaferri 1996). While DR Oct is variable, no photometric period has been reported. It appears that among the Ottmann et al. (1997) Pop II binaries, DR Oct may be the most similar analog to V474 Car, with its retrograde galactic orbit and its X-ray-luminous, evolved, Li-rich G-type primary.

Starting in 1981, Latham, Carney, and collaborators conducted a long-term spectroscopic and radial velocity survey of high proper motion stars, many of which are halo stars. Among the spectroscopic binaries reported by Latham et al. (2002), they showed that the transition between apparently tidally-locked ( $e \simeq 0$ ) tight binaries and the “normal” wide-separation binaries with a wide range of eccentricities appears near orbital period  $\sim 20$  days. V474 Car’s zero eccentricity orbit is consistent with the  $P < 20$  day binary population observed by Latham et al. (2002). Among the 15 single-lined spectroscopic binaries from Latham et al. (2002) with orbital periods of  $< 20$  days, only one has space velocity of  $> 200 \text{ km s}^{-1}$  according to Carney et al. (1994). That star is G 65-22 (HIP 68527, LHS 2846, Ross 838), the primary of which is an unevolved  $\sim 0.6 M_{\odot}$  dwarf with  $[\text{m}/\text{H}] \simeq -1.72$ . Goldberg et al. (2002) identified 34 double-lined spectroscopic binaries among the Carney-Latham sample. Of these, only two had orbital periods of  $< 20$  days and space velocity from Carney et al. (1994) of  $> 200 \text{ km s}^{-1}$  (G 66-59, G 183-9), and the primaries for both systems are, again, unevolved metal-poor  $\sim 0.6 M_{\odot}$  dwarfs. Hence, the Carney-Latham sample of halo stars contains a few rare examples of metal-poor, tight binaries that are *dwarfs*, but no evolved specimens like V474 Car.

Carney et al. (2005) found that while halo and disk stars have surprisingly similar binary frequencies and distributions of orbital parameters, there is a significant difference between the binary frequency of halo stars in prograde orbits ( $\sim 27\%$ ) versus those in retrograde orbits ( $\sim 11\%$ ; like V474 Car). Carney et al. (2005) proposed that given the difference in binarity may be due to the retrograde population containing a significant population of stars from an object (perhaps  $\omega$  Cen?) that was captured by the Milky Way. If so, V474 Car may be a rare binary member of this purportedly accreted population.

V474 Car’s Galactic orbit is notable for its extreme eccentricity. In the Geneva-Copenhagen survey of F/G-type stars in the solar neighborhood (Holmberg et al. 2009), only nine of the 16,682 stars (0.05%) in the survey have an eccentricity greater than or equal to that of V474 Car, and only six of the 16,682 (0.04%) have a smaller perigalacticon. None of those stars, however, are detected in X-rays in the ROSAT All-Sky Survey Bright Source Catalog (Voges et al. 1999) or Faint Source Catalog (Voges et al. 2000). All of those stars are metal poor ( $-2.30 < [\text{Fe}/\text{H}] < -0.88$ ), as is V474 Car ( $[\text{Fe}/\text{H}] \simeq -1.0$ ; §3.5).

## 5. Summary

We have presented a robust analysis of V474 Car, a rare metal poor ( $[\text{Fe}/\text{H}] \simeq -1.0$ ) RS CVn binary with halo kinematics. The star was originally selected in a survey for young, nearby stars due to enhanced Li and  $\text{H}\alpha$  emission, however its extreme heliocentric velocity ( $v_r \simeq 264 \text{ km s}^{-1}$ ) was the first indication that this was no typical pre-MS star. The star is a single-lined spectroscopic binary with evolved G-type primary and a probable K/M-type secondary with orbital period synchronous with the photometrically-constrained rotational period of the primary ( $P \simeq 10.3$  days). The ASAS light curve of the primary also manifests a modulation with a  $\sim 6$  year period and  $\sim 0.1$  mag amplitude, perhaps due to a long-term activity cycle. The star has an eccentricity for its Galactic orbit surpassed by only  $< 0.05\%$  of F/G-type field stars, and its orbit is mildly retrograde ( $V_{\text{helio}} = -241 \text{ km s}^{-1}$ ). The star has few peers, with CD-48 1741 and DR Oct being perhaps the closest analogs as rare halo RS CVns. Its X-ray luminosity and hardness of soft X-ray emission as measured by ROSAT appears similar to that of normal disk RS CVn stars. V474 Car may become an important target for studying the effects of low metallicity on stellar coronae and stellar activity cycles.

E.B. would like to thank Jeremy King for useful discussions regarding the abundance analysis. Thanks also go to Peter Teuben for technical assistance with NEMO. We thank Andrej Prsa and Scott Engle for discussions about the ASAS data, David Cohen for discussion about the ROSAT data, and the anonymous referee for suggestions which improved the paper. E.J. gratefully acknowledges the support of NSF grant AST-0307830. E.B. and E.M. acknowledge support from the University of Rochester School of Arts and Sciences. Stony Brook University is a member of the SMARTS Consortium, which operates the SMARTS observatory on Cerro Tololo.

## REFERENCES

- Ardeberg, A., & Lindgren, H. 1991, *A&A*, 244, 310
- Balachandran, S., Carney, B. W., Fry, A. M., Fullton, L. K., & Peterson, R. C. 1993, *ApJ*, 413, 368
- Barnes, T. G., & Evans, D. S. 1976, *MNRAS*, 174, 489
- Barrado y Navascues, D., Fernandez-Figueroa, M. J., Garcia Lopez, R. J., de Castro, E., & Cornide, M. 1997, *A&A*, 326, 780
- Bubar, E. J., & King, J. R. 2010, *AJ*, 140, 293
- Carlsson, M., Rutten, R. J., Bruls, J. H. M. J., & Shchukina, N. G. 1994, *A&A*, 288, 860
- Carney, B. W., Latham, D. W., Laird, J. B., & Aguilar, L. A. 1994, *AJ*, 107, 2240
- Carney, B. W., Aguilar, L. A., Latham, D. W., & Laird, J. B. 2005, *AJ*, 129, 1886

- Cutri, R. M., et al. 2003, The IRSA 2MASS All-Sky Point Source Catalog, NASA/IPAC Infrared Science Archive. <http://irsa.ipac.caltech.edu/applications/Gator/>,
- Dehnen, W., & Binney, J. 1998, MNRAS, 294, 429
- Demarque, P., Woo, J.-H., Kim, Y.-C., & Yi, S. K. 2004, ApJS, 155, 667
- Dempsey, R. C., Linsky, J. L., Fleming, T. A., & Schmitt, J. H. M. M. 1993, ApJS, 86, 599
- Eker, Z., et al. 2008, MNRAS, 389, 1722
- Fleming, T. A., Schmitt, J. H. M. M., & Giampapa, M. S. 1995, ApJ, 450, 401
- Fleming, T. A., & Tagliaferri, G. 1996, ApJ, 472, L101
- Flower, P. J. 1996, ApJ, 469, 355
- Fuhrmann, K. 1998, A&A, 330, 626
- Goldberg, D., Mazeh, T., Latham, D. W., Stefanik, R. P., Carney, B. W., & Laird, J. B. 2002, AJ, 124, 1132
- Gontcharov, G. A. 2006, Astronomical and Astrophysical Transactions, 25, 145
- Gudehus, D. H. 2001, BAAS, 33, 850
- Høg, E., et al. 2000, A&A, 355, L27
- Holmberg, J., Nordström, B., & Andersen, J. 2009, A&A, 501, 941
- Jensen, E. L. N. et al., in preparation
- Kazarovets, E. V., Samus, N. N., Durlevich, O. V., Frolov, M. S., Antipin, S. V., Kireeva, N. N., & Pastukhova, E. N. 1999, Information Bulletin on Variable Stars, 4659, 1
- King, J. R., Deliyannis, C. P., Hiltgen, D. D., Stephens, A., Cunha, K., & Boesgaard, A. M. 1997, AJ, 113, 1871
- Latham, D. W., Stefanik, R. P., Torres, G., Davis, R. J., Mazeh, T., Carney, B. W., Laird, J. B., & Morse, J. A. 2002, AJ, 124, 1144
- Lockwood, G. W., Skiff, B. A., Henry, G. W., Henry, S., Radick, R. R., Baliunas, S. L., Donahue, R. A., & Soon, W. 2007, ApJS, 171, 260
- Luyten, W. J. 1979, NLTT catalog. Volume I. +90 to +30. Volume II. +30 to 0., by Luyten, W. J. Publ. by Univ. Minnesota, Minneapolis, USA. Vol. I: 282 p., Vol. II: 286 p.,
- Maceroni, C., & van't Veer, F. 1996, A&A, 311, 523

- Makarov, V. V. 2007, *ApJS*, 169, 105
- Morel, T., Micela, G., Favata, F., & Katz, D. 2004, *A&A*, 426, 1007
- Neuhäuser, R., Sterzik, M. F., & Schmitt, J. H. M. M. 1995, *Ap&SS*, 224, 93
- Ottmann, R., Fleming, T. A., & Pasquini, L. 1997, *A&A*, 322, 785
- Padgett, D. L. 1996, *ApJ*, 471, 847
- Perryman, M. A. C., et al. 1997, *A&A*, 323, L49
- Pojmanski, G., Pilecki, B., & Szczygiel, D. 2005, *Acta Astronomica*, 55, 275
- Ramírez, I., Allende Prieto, C., & Lambert, D. L. 2007, *A&A*, 465, 271
- Röser, S., Schilbach, E., Schwan, H., Kharchenko, N. V., Piskunov, A. E., & Scholz, R.-D. 2008, *A&A*, 488, 401
- Rucinski, S. M., & Duerbeck, H. W. 1997, *Hipparcos - Venice '97*, 402, 457
- Ryan, S. G., & Deliyannis, C. P. 1998, *ApJ*, 500, 398
- Schuler, S. C., King, J. R., Terndrup, D. M., Pinsonneault, M. H., Murray, N., & Hobbs, L. M. 2006, *ApJ*, 636, 432
- Snedden, C. A. 1973, Ph.D. Thesis,
- Snider, S., Allende Prieto, C., von Hippel, T., Beers, T. C., Sneden, C., Qu, Y., & Rossi, S. 2001, *ApJ*, 562, 528
- Soderblom, D. R., Pendleton, J., & Pallavicini, R. 1989, *AJ*, 97, 539
- Spite, M., Pasquini, L., & Spite, F. 1994, *A&A*, 290, 217
- Torres, C. A. O., Quast, G. R., da Silva, L., de La, R. R., Melo, C. H. F., & Sterzik, M. 2006, *VizieR Online Data Catalog*, 346, 695
- Teuben, P. 1995, *Astronomical Data Analysis Software and Systems IV*, 77, 398
- van Leeuwen, F. 2007, *Astrophysics and Space Science Library*, 350,
- Voges, W., et al. 1999, *A&A*, 349, 389
- Voges, W., et al. 2000, *IAU Circ.*, 7432, 1
- Zacharias, N., et al. 2010, *AJ*, 139, 2184

Table 5. Abundances for V474 Car

Element	[X/H]	[X/Fe]
Fe	−0.99	0.00
O	−0.39	0.64
Na	−1.23	−0.24
Mg	−0.72	0.27
Si	−1.01	−0.02
Ca	−0.55	0.44
Ti I	−0.44	0.55
Ti II	−0.88	0.11
Mn	−1.45	−0.46
Ni	−1.13	−0.14
Y	−1.17	−0.18
Ba	−1.06	−0.07

Table 6. Atomic Data

Wavelength (Å)	Ion	$\chi$ (eV)	$\log gf$	EQW <sub>⊙</sub> (mÅ)	LogN <sub>⊙</sub>	EQW <sub>v474</sub> (mÅ)	logN <sub>v474</sub>
5054.640	Fe I	3.64	-1.920	42.4	7.42	21.2	6.48
5067.160	Fe I	4.22	-0.970	60.9	7.37	52.2	6.68
5090.780	Fe I	4.26	-0.400	90.9	7.34	68.1	6.36
5109.660	Fe I	4.30	-0.980	77.9	7.74	40.9	6.61
5127.370	Fe I	0.91	-3.310	95.3	7.29	94.0	5.96
5242.490	Fe I	3.63	-0.970	84.0	7.27	61.1	6.16
5307.360	Fe I	1.61	-2.990	87.7	7.46	97.8	6.46
5373.700	Fe I	4.47	-0.760	64.4	7.43	32.7	6.42
5386.340	Fe I	4.15	-1.670	27.9	7.33	4.7	6.04
5398.280	Fe I	4.44	-0.630	71.5	7.39	50.3	6.53
5505.880	Fe I	4.42	-1.300	56.6	7.78	15.8	6.52
5506.780	Fe I	0.99	-2.800	122.1	7.26	179.9	6.68
5554.880	Fe I	4.55	-0.440	99.6	7.71	47.8	6.41
5576.090	Fe I	3.43	-1.000	118.7	7.61	88.3	6.30
5852.220	Fe I	4.55	-1.230	40.4	7.51	20.1	6.69
5855.080	Fe I	4.61	-1.480	19.6	7.34	8.2	6.57
5856.090	Fe I	4.29	-1.330	33.8	7.23	11.3	6.23
5859.590	Fe I	4.55	-0.300	73.6	7.17	30.5	5.99
5862.360	Fe I	4.55	-0.060	84.4	7.11	49.5	6.04
5956.690	Fe I	0.86	-4.600	59.1	7.62	59.2	6.68
6003.010	Fe I	3.88	-1.120	85.9	7.62	56.2	6.48
6065.480	Fe I	2.61	-1.530	112.0	7.28	119.5	6.32
6151.620	Fe I	2.18	-3.300	49.3	7.44	49.3	6.70
6170.500	Fe I	4.79	-0.440	77.2	7.56	46.7	6.62
6173.340	Fe I	2.22	-2.880	66.1	7.39	57.0	6.42
6213.430	Fe I	2.22	-2.480	82.1	7.32	90.1	6.44
6216.360	Fe I	4.73	-1.420	35.7	7.76	33.8	7.34
6219.280	Fe I	2.20	-2.430	89.0	7.38	97.6	6.46
6232.640	Fe I	3.65	-1.220	82.8	7.43	51.7	6.25
6246.320	Fe I	3.60	-0.730	119.3	7.45	110.9	6.47
6252.550	Fe I	2.40	-1.690	118.8	7.32	115.4	6.18
6256.360	Fe I	2.45	-2.410	87.6	7.57	91.9	6.64

Table 6—Continued

Wavelength (Å)	Ion	$\chi$ (eV)	$\log gf$	EQW <sub>☉</sub> (mÅ)	LogN <sub>☉</sub>	EQW <sub>v474</sub> (mÅ)	logN <sub>v474</sub>
6265.130	Fe I	2.17	-2.550	84.1	7.37	95.4	6.52
6290.970	Fe I	4.73	-0.780	73.3	7.79	73.3	7.24
6322.690	Fe I	2.59	-2.430	73.4	7.45	65.6	6.48
6336.820	Fe I	3.68	-0.910	108.4	7.54	86.2	6.41
6344.150	Fe I	2.43	-2.920	67.1	7.65	47.3	6.55
6393.610	Fe I	2.43	-1.570	122.7	7.27	119.2	6.13
6411.650	Fe I	3.65	-0.590	140.0	7.55	103.2	6.27
6498.940	Fe I	0.96	-4.700	43.5	7.47	56.1	6.82
6533.940	Fe I	4.56	-1.380	60.2	8.01	9.2	6.45
6592.910	Fe I	2.73	-1.470	119.5	7.38	107.0	6.18
6593.870	Fe I	2.43	-2.420	82.5	7.43	77.8	6.43
6609.110	Fe I	2.56	-2.690	68.3	7.55	37.2	6.30
6733.150	Fe I	4.64	-1.580	24.0	7.55	11.2	6.82
6750.150	Fe I	2.42	-2.620	70.4	7.37	74.2	6.56
6786.860	Fe I	4.19	-2.070	21.5	7.55	5.2	6.47
7130.920	Fe I	4.22	-0.790	96.2	7.67	66.8	6.59
7284.840	Fe I	4.14	-1.750	42.3	7.61	21.7	6.75
7285.270	Fe I	4.61	-1.700	43.0	8.02	43.2	7.60
7583.790	Fe I	3.01	-1.890	77.7	7.29	61.1	6.27
7879.750	Fe I	5.03	-1.650	39.4	8.27	8.9	7.14
6084.110	Fe II	3.20	-3.800	20.0	7.47	6.0	6.40
6149.250	Fe II	3.89	-2.880	35.0	7.60	8.0	6.33
6238.390	Fe II	3.89	-2.750	47.0	7.75	17.0	6.57
6247.560	Fe II	3.89	-2.440	53.0	7.57	21.0	6.37
6369.460	Fe II	2.89	-4.230	19.0	7.57	7.0	6.57
6456.380	Fe II	3.90	-2.070	66.0	7.49	33.0	6.27
6300.310	O I	0.00	-9.72	5.6	8.68	23.9	8.22
7771.940	O I	9.15	0.37	70.0	8.72	38.3	8.51
7774.170	O I	9.15	0.22	56.7	8.67	22.6	8.29
7775.390	O I	9.15	0.00	49.1	8.74	14.5	8.24
5688.190	Na I	2.11	-0.42	116.9	6.26	47.6	5.03
5711.090	Mg I	4.35	-1.83	106.3	7.66	87.0	6.94

Table 6—Continued

Wavelength (Å)	Ion	$\chi$ (eV)	$\log gf$	EQW <sub>⊙</sub> (mÅ)	LogN <sub>⊙</sub>	EQW <sub>v474</sub> (mÅ)	logN <sub>v474</sub>
5684.490	Si I	4.95	-1.55	57.1	7.41	25.5	6.55
5690.430	Si I	4.93	-1.77	56.6	7.61	14.0	6.44
6155.130	Si I	5.62	-0.78	79.9	7.49	27.4	6.49
6161.297	Ca I	2.52	-1.27	66.6	6.4	61.8	5.81
6166.439	Ca I	2.52	-1.14	67.2	6.28	58.0	5.63
6455.600	Ca I	2.52	-1.50	57.4	6.46	54.2	5.93
6499.650	Ca I	2.52	-1.00	82.1	6.37	96.1	5.94
5978.541	Ti I	1.87	-0.50	22.7	4.88	25.9	4.41
6126.216	Ti I	1.07	-1.43	23.0	5.02	36.8	4.65
6258.706	Ti I	1.46	-0.24	74.0	5.23	90.8	4.59
6261.098	Ti I	1.43	-0.48	50.9	4.99	61.2	4.43
6743.122	Ti I	0.90	-1.63	14.7	4.76	34.7	4.6
6491.561	Ti II	2.06	-1.79	40.8	4.89	29.9	4.01
6491.582	Ti II	2.06	-2.15	40.8	5.25	29.9	4.37
6013.530	Mn I	3.07	-0.25	76.1	5.49	36.3	4.18
6016.670	Mn I	3.08	-0.10	90.5	5.61	36.5	4.05
6021.800	Mn I	3.08	0.03	94.2	5.53	46.3	4.06
6086.280	Ni I	4.26	-0.51	42.3	6.26	11.5	5.11
6175.370	Ni I	4.09	-0.53	53.8	6.34	24.5	5.32
6482.810	Ni I	1.93	-2.97	42.8	6.44	15.1	5.16
6643.640	Ni I	1.68	-2.01	94.2	6.23	84.8	5.02
6772.320	Ni I	3.66	-0.98	47.4	6.23	23.4	5.26
5200.413	Y II	0.99	-0.57	46.3	2.37	31.5	1.2
5853.690	Ba II	0.60	-1.00	63.7	2.25	78.2	1.25
6141.730	Ba II	0.70	-0.07	110.6	2.27	130.2	1.11
6496.910	Ba II	0.60	-0.41	94.1	2.21	122.7	1.19

Note. — Online Table: Line data